TRPM4 conductances in thalamic reticular nucleus neurons generate persistent firing during slow oscillations

Abbreviated title: TRPM4 mediates PF in TRN

John J. O'Malley[1,2], Frederik Seibt[1], Jeannie Chin[3], and Michael Beierlein[1,2]

[1]Department of Neurobiology & Anatomy, McGovern Medical School at UTHealth

Houston, TX 77030

[2]MD Anderson Cancer Center UTHealth Graduate School of Biomedical Sciences,

Houston, TX 77030

Department of Neuroscience, Baylor College of Medicine

Houston, TX 77030

Address for Correspondence

Michael Beierlein
Department of Neurobiology & Anatomy
McGovern Medical School
6431 Fannin Street, Suite 7.046
Houston, TX 77030
Email: michael.beierlein@uth.tmc.edu

Number of pages: 43
Number of figures: 7
Abstract: 246 words
Introduction: 580 words
Discussion: 1255 words

Conflict of interests: The authors declare no competing financial interests.

Acknowledgments: Supported by funds from the Harry S. and Isabel C. Cameron Foundation (J.O.), the Neurodegeneration Consortium and the Belfer Family Foundation (J.C. and M.B.), NIH NS085171, NS086965 (J.C.), and NIH NS077989 (M.B.). We thank Michael Zhu and Oleh Pochynyuk for help with mouse models, John Magnotti for statistical advice and Fabricio Do Monte for helpful discussions.

Abstract

During slow-wave sleep (SWS) and anesthesia, thalamocortical networks generate slow (< 1 Hz) oscillations, with activity in individual neurons showing rhythmic fluctuations between Up and Down States. Neocortical Up states are driven by persistent synaptic activity in recurrent networks. In contrast, rhythmic up states in thalamic neurons are thought to be primarily mediated by cell-intrinsic mechanisms, with postsynaptic Group 1 metabotropic glutamate receptor (mGluR) activation leading to the generation of long-lasting plateau potentials mediated by both T-type Ca^{2+} currents and calcium-activated nonselective cation currents (I_{CAN}). However, the molecular identity of I_{CAN} and the role of thalamic synaptic networks in generating slow oscillations remain unclear. By performing recordings in thalamic slices derived from adult mice of either sex, we observed robust slow oscillatory network activity that did not require mGluR signaling but was completely eliminated in the absence of fast glutamatergic signaling. We found that thalamic glutamatergic inputs triggered persistent firing (PF) in neurons of the thalamic reticular nucleus (TRN). For about 30% of TRN neurons, PF could also be evoked by brief depolarizing steps, while the remaining neurons displayed burst firing. PF was driven by long-lasting plateau potentials that were triggered by Ca^{2+} influx through T-type Ca^{2+} channels and mediated by Ca^{2+} and voltage-dependent transient receptor potential melastatin 4 (TRPM4) channels. Taken together, our results suggest that slow oscillatory activity in TRN neurons typical for SWS is mediated by cell-intrinsic mechanisms that generate PF, and synaptic networks interconnecting TRN with thalamic relay nuclei that generate rhythmicity.

Significance Statement

Slow-wave sleep (SWS) is essential for memory consolidation and efficient removal of potentially toxic metabolites. During SWS, thalamic neurons display slow rhythmic activity, and fluctuate between periods of sustained activity and complete quiescence. The cellular and network contributions to slow thalamic oscillations remain poorly understood. We found that, in thalamic slice preparations of adult mice, thalamic reticular nucleus (TRN) neurons show spontaneous slow oscillations accompanied by persistent firing (PF). While thalamic synaptic networks were critical for oscillatory activity, T-type Ca^{2+} and TRPM4 channels in TRN neurons were responsible for initiation and maintenance of PF, respectively. Our findings help to elucidate the mechanisms involved in TRN oscillatory activity during SWS.

Introduction

A defining feature of natural sleep and anesthesia are slow (< 1Hz) and synchronized rhythms in the thalamocortical system. Rather than acting as a “default state” in the absence of behaviorally relevant sensory inputs, slow oscillations during sleep are thought to be critical for the grouping of higher frequency activity such as sleep spindles (Lüthi, 2014), network plasticity and memory consolidation (Steriade & Timofeev, 2003; Diekelmann & Born, 2010), and for homeostatic processes including the clearance of metabolites (Varga et al., 2016). On a cellular level, slow oscillations are characterized by rapid transitions between periods of sustained depolarizations (Up states) and quiescence (Down states), in both neocortex (Steriade et al., 1993b; Sanchez-Vives and McCormick, 2000) and thalamus (Steriade et al., 1993a; Crunelli and Hughes, 2010). In neocortex, slow oscillations result from activity in extensively interconnected networks of excitatory neurons, leading to long-lasting, rhythmic barrages of synaptic activity which are highly synchronous across large neuronal populations (Sanchez-Vives & McCormick, 2000). It was originally assumed that slow oscillations initiate in neocortex and then spread to thalamic targets (Steriade et al., 1993a). Neocortical slow oscillations persist

55 in the absence of thalamic inputs (Steriade et al., 1993c; Sanchez-Vives and McCormick, 2000)
56 and can entrain thalamic activity through extensive corticothalamic projections (Stroh et al.,
57 2013). However, there is accumulating evidence indicating that thalamic circuits can generate
58 different types of oscillations, which in turn shape cortical activity (Rigas & Castro-Alamancos,
59 2007; Lemieux et al., 2014; Halassa et al., 2011; David et al., 2013; Fernandez et al., 2018).
60 One well-established form of rhythmic activity initiating in the thalamus are sleep spindles (7-14
61 Hz), produced by the reciprocal synaptic interactions of two populations of neurons that show
62 bursting activity during sleep, thalamocortical relay cells and inhibitory thalamic reticular nucleus
63 (TRN) neurons (Beenhakker & Huguenard, 2009). The cellular and network mechanisms that
64 underlie slower forms of thalamic oscillatory activity seen during SWS are not clearly defined
65 (Crunelli and Hughes, 2010). In contrast to neocortex, slow rhythms in the isolated thalamus are
66 not assumed to require synaptic networks but instead are thought to be generated by cell-
67 intrinsic mechanisms (Hughes et al., 2002; Blethyn et al., 2006). For both TRN and thalamic
68 relay cells, activation of postsynaptic Group I mGluRs by either exogenous agonists or high
69 frequency corticothalamic activity results in an increase in excitability, due to the closure of a K^+
70 leak conductance. This enables low threshold Ca^{2+} currents (I_T) and Ca^{2+}-activated non-
71 selective cation currents (I_{CAN}) to generate long-lasting and rhythmic plateau potentials, which in
72 TRN neurons lead to persistent firing (Blethyn et al., 2006). However, the precise role of I_T and
73 the molecular mechanisms mediating I_{CAN} are not known (Zylberberg & Strowbridge, 2017;
74 Crunelli et al., 2018). Furthermore, the requirements for both corticothalamic and intra-thalamic
75 synaptic activity in generating slow thalamic oscillations remain unclear.
76 Here we addressed these questions by performing recordings in horizontal slices of
77 somatosensory thalamus of adult mice. Surprisingly, we observed highly robust slow oscillatory
78 thalamic network activity in the absence of mGluR activation. However, slow oscillations were
79 completely eliminated by antagonists for fast synaptic transmission. We found that a significant
80 number of TRN neurons displayed synaptically-evoked persistent firing (PF), which could also

be evoked by brief depolarizing current steps in the absence of synaptic signaling. PF was triggered by Ca^{2+} influx through T-type Ca^{2+} channels and generated by long-lasting plateau potentials mediated by TRPM4 conductances. Our findings highlight how intrinsic properties of TRN neurons and intra-thalamic synaptic networks interact to generate slow thalamic oscillatory activity.

Materials and Methods:

Animals. We employed C57BL6/J mice (JAX Laboratories, Stock No: 000664) unless specified otherwise. For some experiments, we used TRPC1,4,5,6 general quadruple knockout mice (Sachdeva et al., 2018) kindly provided by Dr. Michael Zhu or TRPC3 general knockout mice (Hartmann et al., 2008) kindly provided by Dr. Oleh Pochynyuk. To optogenetically activate cholinergic inputs to TRN, we used bacterial artificial chromosome (BAC)-transgenic mice expressing channelrhodopsin (ChR2) under the control of the choline acetyltransferase (ChAT) promoter (ChAT–ChR2–EYFP; JAX Laboratories, Stock No: 014546, Zhao et al., 2011). All animals used in this study were treated following procedures in accordance with National Institutes of Health guidelines and approved by the University of Texas Health Science Center at Houston (UTHealth) animal welfare committee.

Slice Preparation. Brain slices derived from adult animals (P90-120) were prepared as described previously (Ting et al., 2014). Briefly, male or female mice were anesthetized using isoflurane and perfused using an ice cold N-Methyl-D-Glutamine (NMDG) based solution saturated with 95% O_2–5% CO_2 consisting of the following (in mM): 92 NMDG, 2.5 KCl, 1.25 NaH_2PO_4, 10 $MgSO_4$, 0.5 $CaCl_2$, 30 $NaHCO_3$, 20 glucose, 20 HEPES, 2 thiouera, 5 Na-ascorbate, and 3 Na-pyruvate. Brains were removed and horizontal slices (300 μm) were cut in ice-cold NMDG-based solution using a VT1200 S vibratome (Leica). Slices were then held in

106 NMDG-based solution maintained at 35°C for ~12 minutes before being transferred to a
107 modified artificial cerebrospinal fluid (ACSF) held at room temperature, consisting of the
108 following (in mM): 92 NaCl, 2.5 KCl, 1.25 NaH_2PO_4, 2 $MgSO_4$, 2 $CaCl_2$, 30 $NaHCO_3$, 25 glucose,
109 20 HEPES, 2 thiouera, 5 Na-ascorbate, and 3 Na-pyruvate. Slices from younger animals (P13-
110 38) were prepared as described previously (Agmon & Connors, 1991). Briefly, mice were
111 anesthetized using isoflurane and then decapitated. Slices were cut in ice-cold cutting solution
112 saturated with 95% O_2/5% CO_2 consisting of the following (in mM): 213.4 sucrose, 2.5 KCl, 1.25
113 NaH_2PO_4, 10 $MgSO_4$, 0.5 $CaCl_2$, 26 $NaHCO_3$, and 11 glucose. Slices were then transferred to
114 ACSF consisting of the following (in mM): 126 NaCl, 2.5 KCl, 1.25 NaH_2PO_4, 2 $MgCl_2$, 2 $CaCl_2$,
115 26 $NaHCO_3$ and 10 glucose, incubated at 35°C for 20 minutes and then held at room
116 temperature until used for experiments.
117
118 *Electrophysiological Recordings.* Recordings were performed in a chamber perfused with
119 ACSF held at 32-34°C using a Warner Instruments TC-324B in-line heater. Cells were
120 visualized via infrared differential interference contrast (IR-DIC) under an Olympus BX51WI
121 microscope equipped with a Dage-MTI IR-1000 camera. Whole-cell recordings were obtained
122 using glass pipettes with a tip resistance of 3-5 MΩ. For current clamp recordings, we used a
123 potassium-based internal solution consisting of (in mM): 133 K-Gluconate, 1 KCl, 2 $MgCl_2$, 0.16
124 $CaCl_2$, 10 HEPES, 0.5 EGTA, 2 Mg-ATP, and 0.4 Na-GTP (adjusted to 290 mOsm and pH 7.3).
125 For voltage clamp recordings of inhibitory postsynaptic currents in neurons of the ventrobasal
126 nucleus of the thalamus (VB), recording pipettes were filled with a cesium-based internal
127 solution consisting of (in mM): 120 $CsMeSO_3$, 1 $MgCl_2$, 1 $CaCl_2$, 10 CsCl, 10 HEPES, 3 QX-314,
128 11 EGTA, 2 Mg-ATP, and 0.3 Na-GTP (adjusted to 295 mOsm and pH 7.3). For loose-patch
129 recordings, 3-5 MΩ pipettes were filled with ASCF. To probe oscillatory network activity,
130 Glutamine (0.3 mM) was added to the ACSF (Bryant et al., 2009; Pita-Almenar et al., 2014). In
131 some experiments we replaced extracellular NaCl with equimolar NMDG and used an internal

132 solution consisting of (in mM): 133 K-Gluconate, 1 KCl, 4 NaCl, 2 $MgCl_2$, 0.16 $CaCl_2$, 10
133 HEPES, 0.5 EGTA, 2 Mg-ATP, and 0.4 Na-GTP (adjusted to 290 mOsm and pH 7.3). For
134 optogenetic experiments cholinergic afferents were activated using 1 ms pulses of blue light
135 using an LED light source (UHP-T-450-EP, Prizmatix) delivered through a 60x, 0.9 NA water-
136 immersion objective (Olympus) and centered locally in the TRN.
137 NBQX, apamin, nimodopine, nifedopine, TTX, 2-APB, flufenamic acid, 9-phenthranol,
138 glibenclamide, CBA, and atropine were obtained from R&D Systems. ω-conotoxin MVII and
139 TTA-P2 were obtained from Alomone labs. All other chemicals were obtained from Sigma-
140 Aldrich.
141
142 *Data acquisition.* Recordings were made using a Multiclamp 700B amplifier (Molecular
143 Devices), filtered at 3–10 kHz, and digitized at 20 kHz with a 16-bit analog-to-digital converter
144 (Digidata 1440A; Molecular Devices). Data were acquired using Clampex 10.3 software
145 (Molecular Devices) and analyzed using custom macros written in IGOR Pro (Wavemetrics).
146
147 *Experimental design and statistical analysis.* TRN neuronal firing evoked by brief (25 ms)
148 current steps was classified into two groups, bursting and persistent firing (PF), based on the
149 duration of the evoked membrane depolarization measured at half-amplitude (see *Results*).
150 Post-hoc K means cluster analysis confirmed that classification into two clusters explained the
151 largest amount of variance. We used a depolarization duration of 200 ms to distinguish between
152 bursting and PF. Due to rundown of PF in whole-cell mode, data acquisition in the TRN was
153 limited to 3 min following establishment of whole-cell configuration. Pharmacological
154 experiments examining the mechanisms underlying PF were carried out by performing
155 recordings in the presence of a given antagonist under study, and comparing results with
156 recordings performed under control conditions. All data in a given group were collected from
157 slices derived from a minimum of 2 animals and reported as mean ± SEM. All statistical

158 analyses were performed with Prism 7 software. To evaluate significant differences in the
159 proportion of PF between different experimental groups we performed a chi square test, and
160 report results in the following format: degrees of freedom in parentheses, followed by the chi-
161 square value and p value. To test for significant differences in the duration of evoked membrane
162 depolarization between groups of neurons, we performed an unpaired *t*-test and report results
163 as: degrees of freedom in parentheses, followed by *t* value and *p* value. Statistical significance
164 was set at $p < 0.05$ and adjusted for multiple statistical comparisons with a Bonferroni correction
165 to correct for pairwise error and to reduce Type I error.
166

167 **RESULTS**

168

169 **Slow oscillatory activity and persistent firing (PF) in thalamic networks**

170 Following activation of postsynaptic Group I mGluRs, individual neurons in the TRN and the
171 adjacent relay nuclei can generate slow oscillatory responses, reminiscent of thalamic activity
172 during SWS (Blethyn et al., 2006). It remains unclear how thalamic synaptic networks contribute
173 to slow oscillatory activity. To examine this issue, we performed experiments in horizontal
174 thalamic slices derived from adult (> 3 month) mice. We and others have previously employed
175 extracellular or optogenetic synaptic stimulation to trigger transient (<2 s) forms of rhythmic
176 thalamic activity *in vitro* (Huguenard and Prince, 1994; Pita-Almenar et al., 2014). Surprisingly,
177 by performing loose-patch recordings from TRN neurons, we observed spontaneous and highly
178 rhythmic patterns of action potential activity that could last several minutes (n = 47 TRN
179 neurons, n = 17 slices). For 12/47 (26%) of recordings, action potential activity was organized
180 as rhythmic bursting (frequency: 1.9 ± 0.1 Hz, n = 12, Fig. 1A). Interestingly, a second group of
181 recordings (17/47, 36%) revealed rhythmic patterns of sustained action potential activity we
182 termed persistent firing (PF), characterized by an initial high-frequency burst, followed by a long-
183 lasting train of action potentials (duration: 964.9±256.4 ms, average firing frequency: 175±23.4

184 Hz, n = 17, Fig. 1B). For neurons displaying rhythmic PF, oscillation frequency was 0.5 ± 0.1 Hz
185 (n = 17), significantly lower compared to the oscillation frequency of cells showing burst firing
186 ($t(28) = 6.5$, $p = 10^{-16}$; Fig. 1E). The remaining recordings showed more complex patterns of
187 rhythmic activity that included single spikes, bursts and/or PF (n = 18, *data not shown*). These
188 data indicate the presence of two firing modes in the adult TRN, burst firing and PF, which are
189 associated with oscillatory activity at distinct frequencies.

190 Relay neurons in the ventrobasal nucleus (VB) receive their sole inhibitory input from
191 neurons in the TRN. Therefore, the patterns of synaptic inhibitory responses recorded in VB
192 neurons should closely reflect rhythmic spike firing observed in TRN. To confirm this, we
193 performed voltage-clamp recordings from VB neurons at a holding potential of 0 mV to isolate
194 IPSCs. In 76% (n = 22/29) of all VB neurons that showed oscillatory synaptic activity indicative
195 of intact thalamic networks, we recorded synaptic responses organized as long-lasting high-
196 frequency IPSC barrages (duration: 620.1±54.3 ms, n = 32, Fig. 1D) which occurred
197 rhythmically over several minutes (0.5±0.1 Hz, n = 32). A smaller fraction of recordings showed
198 rhythmic IPSC bursts (n = 4, Fig.1C). Thus, relay neurons are the target of persistent inhibition
199 during slow oscillatory activity, likely mediated by TRN neurons with PF.

200 Postsynaptic mGluR activation by exogenous agonists or high-frequency stimulation of
201 glutamatergic afferents can lead to slow oscillatory activity in TRN neurons, even in the absence
202 of fast synaptic signaling (Blethyn et al., 2006). In contrast, by performing whole-cell recordings
203 in TRN, we found that rhythmic patterns of PF did not occur spontaneously but instead were
204 evoked by brief bursts of large-amplitude thalamoreticular EPSPs (Fig. 1F). Furthermore,
205 rhythmic IPSCs recorded in VB cells were fully blocked by bath application of NBQX (n = 5, Fig.
206 1G), suggesting that similar to spindle-like activity (Huguenard and McCormick, 2007), slow
207 oscillatory activity relied on a network of interconnected TRN and relay neurons, at least under
208 our experimental conditions.

209 Anatomic and functional studies have shown considerable axonal divergence for TRN to
210 VB projections, resulting in highly overlapping TRN afferents to neighboring VB neurons
211 (Pinault, 2004; Pita-Almenar et al., 2014). In agreement, the timing and duration of oscillatory
212 IPSC barrages were highly synchronous for VB neuronal pairs recorded simultaneously (Fig.
213 2A). Synchrony was maintained for individual IPSCs throughout the entire barrage suggesting
214 that the large majority of IPSCs were spike-mediated, without a detectable contribution of
215 asynchronous GABA release (Hefft & Jonas, 2005).
216 We found that the majority of VB recordings showed oscillatory IPSC barrages with little
217 variability of the initial IPSC amplitude, consistent with activity of a single presynaptic TRN
218 neuron (Fig. 1C,D). However, some recordings contained two distinct types of barrages, with
219 each barrage showing a distinct initial IPSC amplitude and duration Figs. 1G, 2B,C). These
220 responses are most readily explained as being generated by convergent inputs from two
221 presynaptic TRN neurons with distinct firing patterns, including bursting and PF. Importantly,
222 IPSC bursts and barrages evoked by independent TRN neurons displayed clear rhythmicity but
223 never occurred synchronously. These data confirm our previous findings derived in thalamic
224 slices of less mature animals (Pita-Almenar et al., 2014) and suggest that local thalamic
225 networks can mediate robust oscillatory activity in the absence of widespread synchrony.
226
227 **Brief depolarizations trigger PF in TRN neurons**
228 So far our data indicate that a significant fraction of TRN neurons shows PF during network
229 activity. To better characterize the properties and underlying mechanisms of PF, we performed
230 whole-cell recordings and blocked network activity by adding NBQX to the bath solution. Brief
231 depolarizing current steps (25 ms, 400 pA) from a resting potential of -75 mV generated bursts
232 of action potentials (average number of spikes: 8.1±0.2, n = 74) in 67% of neurons recorded
233 (Fig. 3A). For the remaining neurons (37/111, 33%) we observed sustained action potential
234 activity (average number of spikes: 72.2±9.8; firing frequency: 99.1±7.5 Hz, n = 37) closely

resembling PF observed during network activity. PF was mediated by long-lasting plateau potentials (amplitude from rest: 29.3±0.8 mV, plateau duration: 807.1±41.7 ms, n = 37, Fig. 3A,B) that terminated in a stepwise manner. Using the duration of the current-step evoked membrane depolarization, we performed K means cluster analysis, confirming that TRN firing patterns are most readily classified into two distinct groups, bursting and PF, with the latter group displaying membrane depolarizations of > 200 ms. We found that PF remained stable for several minutes but then decayed over time, regardless of composition of the internal solution (Fig. 3C). Therefore, for the remainder of this study we limited data acquisition to the first 3 minutes in whole-cell mode.

PF occurs late during development and is controlled by SK conductances

Previous studies performed under similar experimental conditions have not reported PF in preparations derived from younger animals (<P30). To determine if PF is developmentally regulated, we carried out additional recordings in slices prepared from mice aged P13-18 and P28-38. Compared to adult mice, only 1/24 (4%) of cells at P13-18 and 1/23 (4%) of cells at P28-38 displayed PF (Fig. 3D-F), indicating that PF is prominent only in fully mature animals.

The generation of plateau potentials that underlie PF is likely to be tightly regulated by K^+ conductances, including small conductance Ca^{2+}-activated K^+ channels (SK). To examine this possibility, we performed recordings in the presence of the SK channel blocker apamin (100 nM). Compared to control conditions, a much larger fraction of TRN cells in adult animals showed PF (92%, n = 46/50 $\chi^2(1) = 47.5$, $p = 10^{-16}$; Fig. 3D-F). Thus, excitatory conductances responsible for PF are widely expressed in the adult TRN but appear to be strongly controlled by SK conductances. Given the role of SK channels in regulating PF in the adult, the developmental increase in PF we observed might be solely mediated by a progressive downregulation of SK conductances. However, we found that even in the presence of apamin the incidence of PF remained very low early in development and dramatically increased with

261 animal age (P13-18: 12%, n = 25, P28-38: 41%, n = 24, P90-120: 92%; Fig. 3D-F), suggesting a
262 developmental upregulation of excitatory mechanisms that underlie PF. Finally, we examined if
263 neurons in the ventrobasal nucleus of the thalamus (VB) displayed plateau potentials in the
264 presence of apamin. In contrast to TRN, PF was completely absent from VB (0/11 cells; *data*
265 *not shown*). Thus, the mechanisms underlying PF do not appear to be uniformly expressed in all
266 thalamic nuclei.
267
268 **Metabotropic glutamate receptor activation is not necessary for PF**
269 Previous work has highlighted a critical role of postsynaptic group I mGluR activation in enabling
270 intrinsic oscillations and Up states in TRN neurons (Blethyn et al., 2006). While PF under our
271 experimental conditions did not require exogenous or synaptic mGluR I activation, it is possible
272 that mGluRs were tonically activated by ambient glutamate (Crabtree et al., 2013) or in a ligand
273 independent manner (Sun et al., 2016). To examine this possibility, we probed TRN firing in the
274 presence of the non-competitive mGluR1 antagonist JNJ 16259685 (JNJ) and the non-
275 competitive mGluR5 antagonist MTEP. Block of group I mGluRs did not significantly change the
276 incidence of PF (Control: 33%, n = 111; JNJ+MTEP: 48%, n = 27, $\chi^2(1) = 1.7$, $p = 0.19$) or the
277 plateau potential duration for cells with PF (Control: 807.1±41.7 ms, JNJ+MTEP: 599.8±64.3
278 ms, $t(46) = 1.85$, $p = 0.071$; Fig. 4A,B). These data suggest that under our experimental
279 conditions Group I mGluR activation is not essential for PF.
280
281 **Activation of T-type calcium channels is required for PF**
282 Next, we examined if PF is voltage-dependent, by evoking action potential activity from
283 two distinct holding potentials. TRN cells held initially at -60 mV never displayed PF or plateau
284 potentials (0/15 cells; Fig. 4C,D). However, when the holding potential was adjusted to -75 mV,
285 8/15 neurons generated PF ($\chi^2(1) = 1.7$, $p = 0.0013$), suggesting that the underlying
286 mechanisms of PF are voltage dependent.

287 To further isolate the mechanisms responsible for PF, we employed a pharmacological
288 approach. Due to the washout of PF in whole-cell mode, it was not possible to quantify changes
289 in PF prior to and following bath application of antagonists for a given neuron. Therefore, we
290 performed all recordings in the presence of a given antagonist and made comparisons to
291 neurons recorded under control conditions (see *Materials and Methods*). To limit the number of
292 recordings required for meaningful statistical comparisons, we performed the following
293 experiments in the presence of apamin, which, as described above, results in PF in 92% of
294 neurons (Fig. 3E,F).
295 Previous studies have indicated that T-type Ca^{2+} channels are critical for the generation
296 of mGluR-dependent Up states (Hughes et al., 2002; Blethyn et al., 2006). The voltage-
297 dependence of PF we observed appears to be consistent with these results. To confirm the
298 involvement of T-type Ca^{2+} channels in generating PF, we performed recordings in the presence
299 of the specific antagonist TTA-P2 (1 μM). Under these conditions, depolarizing current steps still
300 led to action potential firing, but PF was completely eliminated (Apamin: 92%, Apamin+TTA-P2:
301 0%, n = 17, $\chi^2(1) = 46.5$, $p = 10^{-20}$; Fig. 4E,F). Thus, T-type Ca^{2+} channels are required for the
302 generation of PF.
303
304 **The plateau potential underlying PF is mediated by a sodium current**
305 It is possible that long-lasting plateau potentials in TRN neurons are entirely mediated by T-type
306 Ca^{2+} conductances (Zylberberg and Strowbridge, 2017). While these channels show rapid
307 inactivation following strong depolarization, their inactivation is not complete for smaller
308 depolarizations near the resting membrane potential, resulting in a steady-state inward
309 ("window") current (Williams et al., 1997). However, PF observed in the present study was
310 accompanied by large membrane depolarizations that do not appear to be compatible with a
311 significant role of T-type Ca^{2+} channels. Therefore, we systematically examined the possible
312 involvement of other voltage- or Ca^{2+}-gated non-inactivating conductances. We first tested the

313 role of high-threshold Ca^{2+} channels (L, P/Q, and N). In the presence of the selective L-type
314 antagonist Nimodipine (Nim, 20 μM; Fig. 5A) the incidence of PF (Apamin: 92%, Apamin+Nim:
315 80%, n = 10, $\chi^2(1) = 0.3$, $p = 0.6$; Fig. 5B) and plateau potential duration for cells with PF
316 (Apamin: 1108.5±126.6 ms, Apamin+Nim: 846.8±235 ms, $t(48) = 0.9$, $p = 0.38$; Fig. 5C)
317 remained comparable to responses recorded in apamin. Similarly, incubating slices in the P/Q
318 and N antagonist ω-conotoxin MVIIC (ω-Ctx , 1 μM) did not lead to significant changes in the
319 incidence of PF (Apamin: 92%, Apamin+ω-Ctx: 70%, n = 10, $\chi^2(1) = 1.4$, $p = 0.23$; Fig. 5B), and
320 plateau potential duration (Apamin: 1108.5±126.6 ms, Apamin+ω-Ctx: 726.7±196.2 ms, $t(47) =$
321 1.2, $p = 0.24$; Fig. 5C), suggesting that high-threshold Ca^{2+} channels do not play a critical role in
322 PF.

323 It is possible that plateau potentials are mediated by activation of a persistent Na^+
324 current (I_{NAP}) (Kim and McCormick, 1998). We found that in the presence of apamin and TTX
325 (500 nM), fast action potential activity was completely blocked, revealing a plateau potential in
326 9/16 cells (amplitude: 30±1.2 mV, n = 16, Fig. 5A), a smaller fraction compared to conditions in
327 apamin (Apamin: 92%, Apamin+TTX: 56%, $\chi^2(1) =10$, $p = 0.002$; Fig. 5B). Plateau potential
328 duration remained comparable to control (Apamin: 1108.5±126.6 ms, Apamin+TTX:
329 912.8±325.7 ms, $t(49) = 0.7$, $p = 0.5$; Fig. 5C). These data indicate that while action potential
330 activity mediated by transient Na^+ currents or I_{NAP} might facilitate plateau potential generation,
331 neither are strictly required.

332 Next, we examined if Na^+ current flow via conductances other than voltage-gated Na^+
333 channels are essential for plateau potentials, by substituting the majority of extracellular Na^+
334 with NMDG. We found that in the presence of NMDG (together with apamin and TTX) the
335 incidence of plateau potential generation was significantly reduced (apamin + TTX: 56%,
336 apamin + TTX + NMDG: 11%, n = 28, $\chi^2(1) = 10.6$, $p = 0.001$; Fig. 5A-C), suggesting that PF is
337 mediated at least in part by a TTX-insensitive Na^+ current.

338

339 **TRPM4 channels underlie PF in the TRN**

340 Our data thus far are consistent with a role of the Ca^{2+}-activated nonselective cationic current
341 (I_{CAN}) in mediating plateau potentials. Transient receptor potential (TRP) channels have been
342 previously proposed as molecular mechanisms mediating I_{CAN} (Launay et al., 2002), with
343 transient receptor potential canonical (TRPC) and melastatin (TRPM) channels as the most
344 likely candidates. To examine the potential involvement of TRPC channels, we performed
345 recordings in slices derived from global TRPC3 null mutant mice (TRPC3 KO, Hartmann et al.,
346 2008) and from global quadruple TRPC1,4,5,6 null mutant mice (QKO, Tian & Zhu, 2018), in the
347 presence of apamin. For both mouse lines, the incidence of PF (Apamin: 92%, TRPC3 KO:
348 70%, n = 10, $\chi^2(1) = 3.4$, $p = 0.65$; QKO: 70%, n = 10, χ^2 (1) = 3.4, $p = 0.65$; Fig. 6B) and
349 plateau potential duration (Apamin: 1108.5±126.6 ms, TRPC3 KO: 841.1±136 ms, $t(47) = 0.9$, p
350 = 0.39; QKO: 752.6±133.4 ms, $t(47) = 1.1$, $p = 0.27$; Fig. 6C) were comparable to our
351 observations in WT animals, suggesting that at least 5 of the 7 TRPCs known to be expressed
352 in the brain are not involved in mediating PF.

353 Next, we investigated a possible role of TRPM channels in mediating PF. TRPM2 has
354 been shown to facilitate burst firing (Lee et al., 2013), while both TRPM4 and TRPM5 have been
355 implicated in e.g. the generation of plateau potentials in cortex (Lei et al., 2014) and of slow
356 inward currents in cerebellar Purkinje cells (Kim et al., 2013). We found that in the presence of
357 the broad spectrum TRP channel inhibitor flufenamic acid (FFA, 100 μM), PF was completely
358 eliminated (Apamin: 92%, Apamin+FFA: 0%, n = 17, $\chi^2(1) = 46.6$, $p = 10^{-20}$; Fig. 6A-C). Next, we
359 examined the effects of the broad-spectrum inhibitor 2-Aminoethoxydiphenyl borate (2-APB)
360 which among TRP channels blocks TRPC7 and TRPM2, but does not inhibit TRPM4 or TRPM5.
361 2-APB had no effect on PF (Apamin: 92%, Apamin+ 2-APB: 90%, n = 10, $\chi^2(1) = 0.4$, $p = 0.54$;
362 Fig. 6B), with plateau potential duration comparable to control conditions (Apamin:
363 1108.5±126.6 ms, Apamin+2-APB: 758±132.4 ms, $t(49) = 1.3$, $p = 0.22$; Fig. 6C), ruling out a
364 role of TRPM2 or TRPC7 and suggesting that either TRPM4 or TRPM5 might mediate PF. Both

365 channels are voltage-dependent, monovalent-selective, and require increases in intracellular
366 Ca^{2+} for their activation (Launay et al., 2002; Nilius et al., 2003). We found that in the presence
367 of the TRPM4/5 antagonists 9-Phenthranol (9-Phen, 100 µM) and glibenclamide (Glib, 100 µM)
368 PF was completely eliminated (Apamin: 92%, Apamin+9-Phen: 15%, n = 15, $\chi^2(1) = 34.2$, $p =$
369 10^{-14}; Glib: 0%, n = 21, $\chi^2(1) = 51.4$, $p = 10^{-26}$; Fig. 6B). As both antagonists are known to have
370 non-specific effects, we performed additional experiments using the recently developed
371 selective TRPM4 antagonist 4-Chloro-2-[[2-(2-chlorophenoxy) acetyl]amino]benzoic acid (CBA,
372 Ozhatil et al., 2018). In the presence of CBA (50 µM), cells never displayed PF (Apamin: 92%,
373 CBA: 0%, n = 15, $\chi^2(1) = 44$, $p = 10^{-17}$; Fig. 6A,B). Taken together, our results indicate that
374 TRPM4 conductances mediate the plateau potential underlying PF.
375 Since increases in intracellular Ca^{2+} are required for TRPM4 activation, chelation of Ca^{2+}
376 using exogenous buffers such as BAPTA should eliminate PF. However, due to the rundown of
377 PF, such experiments were not feasible. We therefore probed a possible Ca^{2+} requirement of
378 PF by replacing extracellular Ca^{2+} with equimolar Ba^{2+}. Ba^{2+} passes through T-type Ca^{2+}
379 channels and generates large inward currents (Huguenard & Prince, 1992), but unlike Ca^{2+}
380 does not lead to TRPM4 activation (Nilius et al., 2004; Yamaguchi et al., 2014). Under these
381 conditions, brief depolarizing steps still led to prominent burst firing, indicating that T-type Ca^{2+}
382 channel dependent dendritic depolarizations were not affected (Fig. 6A). However, none of the
383 cells displayed PF (Apamin: 92%, Apamin+Ba^{2+}: 0%, n = 15, $\chi^2(1) = 44$, $p = 10^{-17}$; Fig. 6B,C).
384 These data further confirm that T-type Ca^{2+} channels alone are not sufficient to generate
385 plateau potentials. Instead, our data suggest that T-type Ca^{2+} channel activation and the
386 resulting Ca^{2+} increases lead to the activation of TRPM4 conductances and the generation of
387 PF.
388
389 **Synaptic recruitment of muscarinic acetylcholine receptors suppresses PF**

390 Finally, we examined the modulation of PF by synaptic activity. TRN neurons are the target of
391 cholinergic afferents from the basal forebrain and brainstem (Hallanger and Wainer, 1988). Our
392 previous studies have shown that acetylcholine (ACh) release leads to a biphasic postsynaptic
393 response, with fast excitation mediated by nicotinic ACh receptors (nAChRs) and slow and long-
394 lasting inhibition mediated by M2 muscarinic receptors (mAChRs) coupled G protein-gated
395 inward rectifying K^+ (GIRK) channels (Sun et al., 2013). To examine if cholinergic inputs can
396 trigger PF in the TRN, we performed experiments using BAC-ChAT-ChR2 mice that selectively
397 express ChR2 in cholinergic neurons (Zhao et al., 2011) and optogenetically evoked ACh
398 release with light pulses (1 ms) centered over the recorded neuron. To avoid wash-out of PF,
399 TRN neurons were recorded in loose-patch mode. Under these conditions, 2/5 of neurons
400 displayed PF (Fig. 7A,C). We reasoned that the activation of mAChRs and the resulting GIRK
401 activation might limit the expression of PF. Indeed, following atropine application to block
402 mAChRs, action potential firing was significantly prolonged in all neurons recorded (Control:
403 213.5±94 ms, Atropine: 416.3±84.1 ms, $t(4) = 7.1$, $p = 0.002$; Fig. 7A-C), and the incidence of
404 PF increased from 40% to 80%. These data show that mAChRs can modulate the expression of
405 PF.
406

407 **Discussion**

408 Here we have identified TRPM4 as the mechanism underlying PF in adult neurons of the TRN.
409 Furthermore, our data indicate that the large depolarizations and intracellular Ca^{2+} increases
410 required for TRPM4 activation are generated by Ca^{2+} influx through T-type Ca^{2+} channels.
411 Previous studies have focused on cellular pacemakers as being primarily responsible for slow
412 thalamic oscillations. Instead, our findings highlight that intrathalamic networks are equally
413 capable of generating slow rhythmic activity.
414

415 **Mechanisms of PF in the TRN**

416 Our results extend recent work that has implicated TRPM4 in controlling neuronal excitability in
417 cortex (Lei et al., 2014; Riquelme et al., 2018), hippocampus (Menigoz et al., 2016), substantia
418 nigra (Mrejeru et al., 2011), and brainstem (Picardo et al., 2019). A unique feature of TRPM4 is
419 its dependence on both depolarization and large increases in intracellular Ca^{2+} concentration
420 (Launay et al., 2002; Nilius et al., 2003; Nilius et al., 2004). Since dendritic Ca^{2+} signals can
421 experience decay under whole-cell conditions, this might partly explain why we consistently
422 observed rundown of PF in the present study. Alternatively, recordings in whole-cell mode might
423 have led to the dialysis of critical signaling molecules. TRPM4 conductances rapidly desensitize
424 in excised patches (Zhang et al., 2005) and in whole-cell mode, but modulators such as PIP2
425 can restore TRPM4 activity. Additional investigations into the mechanisms of TRPM4 regulation
426 under physiological conditions will be important.

427 What are the Ca^{2+} sources of TRPM4 activation? We found that pharmacological block
428 of T-type Ca^{2+} channel using the specific antagonist TTA-P2 completely eliminated PF. In
429 addition, replacing Ca^{2+} with Ba^{2+} abolished PF. These findings suggest that the Ca^{2+} increases
430 required for TRPM4 activation are mediated by influx through T-type Ca^{2+} channels although we
431 cannot rule out a contribution of R-type Ca^{2+} channels (Zaman et al., 2011) or release from
432 internal stores (Neyer et al., 2016). $Ca_V3.3$ channels mediating I_T are primarily expressed in the
433 distal dendrites of TRN neurons and their activation during burst firing results in large dendritic
434 but more modest somatic Ca^{2+} signals (Crandall et al., 2010; Astori et al., 2011). This would
435 suggest a dendritic location of TRPM4. In this scenario, membrane depolarizations necessary
436 for TRPM4 activation would likely be mediated by synaptically-generated T-type dependent Ca^{2+}
437 spikes, which in contrast to fast Na^+ action potentials, propagate effectively into TRN dendrites
438 (Crandall et al., 2010; Connelly et al., 2015).

439 We found that in the presence of apamin, PF could be observed in most recordings,
440 suggesting that TRPM4 conductances are expressed in the large majority of TRN neurons.
441 Thus, SK channels control both the initiation and duration of PF, likely due to the close

442 functional association between T-type and SK2 channels (Cueni et al., 2008). Similarly, we
443 found that GIRK conductances activated by M2 muscarinic receptors controlled the duration of
444 PF, suggesting that *in vivo* PF is not all-or-none but under constant regulatory control. While PF
445 has been observed in anesthetized preparations (Fuentealba et al., 2005), the activity of a
446 number of modulatory systems converging on TRN might explain why PF has yet to be
447 described during natural sleep.

448 Plateau potentials and PF have been observed in neurons throughout the brain
449 (Zylberberg & Strowbridge, 2017), including in several types of thalamic neurons, though there
450 is no definitive understanding of the underlying mechanisms. In neurons of the anterodorsal
451 thalamus, brief hyperpolarizing steps can lead to persistent firing over several minutes via
452 undefined mechanisms (Kulkarni et al., 2011). In local interneurons of the lateral geniculate
453 nucleus, postsynaptic mGluR5s can trigger long-lasting plateau potentials and PF lasting
454 minutes, possibly via recruitment of TRP conductances (Pressler & Regehr, 2013). For both
455 TRN and thalamic relay neurons in a number of species, group I mGluR activation can trigger
456 rhythmic forms of PF, mediated by the closure of a K^+ leak conductance, allowing the
457 generation of a long-lasting inward current mediated by the non-inactivating portion of T-type
458 Ca^{2+} channel conductance (Hughes et al., 2002; Blethyn et al., 2006). Our present findings differ
459 from these results in four important aspects: First, PF did not require mGluR activation and the
460 resulting closure of K^+ leak conductances. Second, in the absence of mGluR activation, PF did
461 not occur in a cell-intrinsic manner but required fast synaptic inputs. Under our experimental
462 conditions, both cholinergic inputs and bursts of glutamatergic thalamic inputs triggered PF,
463 likely by generating global Ca^{2+} spikes (Connelly et al., 2015). Third, while T-type Ca^{2+} channels
464 were important for the initiation of PF, our results are inconsistent with a critical role of I_T in
465 generating long-lasting currents that lead to plateau potentials. We found that plateau potentials
466 reached levels of ~-45 mV, where T-type Ca^{2+} conductances at steady-state experience near
467 full inactivation. Furthermore, the lack of PF in the presence of Ba^{2+}, which should allow for the

468 generation of a I_T-mediated window current (Huguenard and Prince, 1992) suggests that T-type
469 Ca^{2+} currents alone are unlikely to mediate PF. Fourth, using the potent and selective
470 antagonist CBA (Ozhatil et al., 2018), we showed that I_{CAN} was essential for the generation of
471 plateau potentials and was mediated by TRPM4. It should be stated that the majority of TRP
472 antagonists employed in previous studies have a number of non-specific effects, so the
473 validation of CBA as a selective TRPM4 antagonist under our experimental conditions will
474 require independent confirmation in additional studies.
475
476 **Mechanisms of slow thalamic oscillations**
477 Accumulating evidence indicates that both cortex and thalamus can generate oscillations in
478 isolation, suggesting that rhythmic activity in the intact thalamocortical system results from the
479 complex interplay of multiple distinct oscillators (Crunelli and Hughes, 2010). While there has
480 been extensive research on the cortical mechanisms mediating slow rhythms, the nature of
481 thalamic pacemakers are less well understood (Neske, 2016). Previous work has shown that
482 both TRN and relay neurons are capable of generating cell-intrinsic rhythms in the 1 Hz range,
483 but only under conditions of postsynaptic mGluR activation (Hughes et al., 2002; Blethyn et al.,
484 2006). Under physiological conditions, this would require sustained corticothalamic activity,
485 indicating that both thalamic cell types act as conditional oscillators. Our findings derived from
486 adult thalamic slices highlight an alternative mechanism and suggest that networks of TRN and
487 VB cells can generate robust and long-lasting slow oscillatory activity, in the absence of
488 sustained afferent activity. We observed an inverse relationship between TRN firing duration
489 and oscillatory frequency. It is therefore tempting to suggest that changes in TRN activity as
490 seen during PF acts to reduce the frequency of thalamic oscillations, via recruitment of
491 $GABA_B$Rs (Kim et al., 1997) or extrasynaptic high-affinity $GABA_A$Rs (Herd et al., 2013), thereby
492 changing the latency to rebound burst generation (Schofield et al., 2009). Thus, both intrinsic
493 and network mechanisms might interact to generate thalamic rhythmicity.

494 Our network data suggest that robust thalamic rhythmicity can occur in the absence of
495 precise synchrony, highlighting that both processes can occur independently. While thalamic
496 oscillatory activity is commonly referred to as synchronous (Fogerson and Huguenard, 2016),
497 there have been few studies that have systemically examined the degree of precise thalamic
498 synchronization during distinct behavioral states. We have previously shown that synaptically
499 evoked thalamic oscillatory activity rapidly desynchronizes, due to a number of cellular and
500 network mechanisms, including variable latencies of rebound bursting in relay neurons, TRN-
501 mediated lateral inhibition, and powerful but sparse thalamoreticular connections (Pita-Almenar
502 et al., 2014). Our current data suggest that the heterogeneity in TRN firing might act as an
503 additional factor in preventing synchrony in isolated thalamic networks. As has been suggested
504 previously (Contreras and Steriade, 1996), this would argue that synchrony in thalamic networks
505 is primarily regulated by afferent inputs, particularly from cortex.
506

507 **References:**

508 Agmon A, Connors BW (1991) Thalamocortical responses of mouse somatosensory (barrel)
509 cortex in vitro. Neuroscience 41:365–379 Available at:
510 http://www.ncbi.nlm.nih.gov/pubmed/1870696.

511 Astori S, Wimmer RD, Prosser HM, Corti C, Corsi M, Liaudet N, Volterra A, Franken P, Adelman
512 JP, Lüthi A (2011) The Ca v3.3 calcium channel is the major sleep spindle pacemaker in
513 thalamus. Proc Natl Acad Sci U S A 108:13823–13828.

514 Beenhakker MP, Huguenard JR (2009) Neurons that Fire Together Also Conspire Together: Is
515 Normal Sleep Circuitry Hijacked to Generate Epilepsy? Neuron 62:612–632 Available at:
516 http://dx.doi.org/10.1016/j.neuron.2009.05.015.

517 Blethyn KL, Hughes SW, Tóth TI, Cope DW, Crunelli V (2006) Neuronal basis of the slow (<1
518 Hz) oscillation in neurons of the nucleus reticularis thalami in vitro. J Neurosci 26:2474–
519 2486.

520 Bryant AS, Li B, Beenhakker MP, Huguenard JR (2009) Maintenance of thalamic epileptiform
521 activity depends on the astrocytic glutamate-glutamine cycle. J Neurophysiol 102:2880–
522 2888.

523 Connelly WM, Crunelli V, Errington AC (2015) The global spike: Conserved dendritic properties
524 enable unique ca2+ spike generation in low-threshold spiking neurons. J Neurosci
525 35:15505–15522.

526 Contreras D, Steriade M (1996) Synchronization of low-frequency rhythms in corticothalamic
527 networks. Neuroscience 76:11–24.

528 Crabtree JW, Lodge D, Bashir ZI, Isaac JTR (2013) GABAA, NMDA and mGlu2 receptors
529 tonically regulate inhibition and excitation in the thalamic reticular nucleus. Eur J Neurosci
530 37:850–859.

531 Crandall SR, Govindaiah G, Cox CL (2010) Low-threshold Ca 2+ current amplifies distal
532 dendritic signaling in thalamic reticular neurons. J Neurosci 30:15419–15429.

533 Crunelli V, Hughes SW (2010) The slow (1 Hz) rhythm of non-REM sleep: A dialogue between
534 three cardinal oscillators. Nat Neurosci 13:9–17.

535 Crunelli V, Larincz ML, Connelly WM, David F, Hughes SW, Lambert RC, Leresche N, Errington
536 AC (2018) Dual function of thalamic low-vigilance state oscillations: Rhythm-regulation and
537 plasticity. Nat Rev Neurosci 19:107–118.

538 Cueni L, Canepari M, Luján R, Emmenegger Y, Watanabe M, Bond CT, Franken P, Adelman

539 JP, Lüthi A (2008) T-type Ca2+ channels, SK2 channels and SERCAs gate sleep-related
540 oscillations in thalamic dendrites. Nat Neurosci 11:683–692.

541 David F, Schmiedt JT, Taylor HL, Orban G, Di Giovanni G, Uebele VN, Renger JJ, Lambert RC,
542 Leresche N, Crunelli V (2013) Essential thalamic contribution to slow waves of natural
543 sleep. J Neurosci 33:19599–19610.

544 Diekelmann S, Born J (2010) The memory function of sleep. Nat Rev Neurosci 11:114–126
545 Available at: http://dx.doi.org/10.1038/nrn2762.

546 Fernandez LMJ, Vantomme G, Osorio-Forero A, Cardis R, Béard E, Lüthi A (2018) Thalamic
547 reticular control of local sleep in mouse sensory cortex. Elife 7:1–25.

548 Fogerson PM, Huguenard JR (2016) Tapping the Brakes: Cellular and Synaptic Mechanisms
549 that Regulate Thalamic Oscillations. Neuron 92:687–704 Available at:
550 http://dx.doi.org/10.1016/j.neuron.2016.10.024.

551 Fuentealba P, Timofeev I, Bazhenov M, Sejnowski TJ, Steriade M (2005) Membrane bistability
552 in thalamic reticular neurons during spindle oscillations. J Neurophysiol 93:294–304.

553 Halassa MM, Siegle JH, Ritt JT, Ting JT, Moore CI (2011) Selective optical drive of thalamic
554 reticular nucleus generates thalamic bursts & cortical spindles. Nat Neurosci 14:1118–
555 1120.

556 Hallanger AE, Wainer BH (1988) Ultrastructure of ChAT-immunoreactive synaptic terminals in
557 the thalamic reticular nucleus of the rat. J Comp Neurol.

558 Hartmann J, Dragicevic E, Adelsberger H, Henning HA, Sumser M, Abramowitz J, Blum R,
559 Dietrich A, Freichel M, Flockerzi V, Birnbaumer L, Konnerth A (2008) TRPC3 Channels Are
560 Required for Synaptic Transmission and Motor Coordination. Neuron 59:392–398.

561 Hefft S, Jonas P (2005) Asynchronous GABA release generates long-lasting inhibition at a
562 hippocampal interneuron-principal neuron synapse. Nat Neurosci 8:1319–1328.

563 Herd MB, Brown AR, Lambert JJ, Belelli D (2013) Extrasynaptic GABAA receptors couple
564 presynaptic activity to postsynaptic inhibition in the somatosensory thalamus. J Neurosci
565 33:14850–14868.

566 Hughes SW, Cope DW, Blethyn KL, Crunelli V (2002) Cellular Mechanisms of the Slow (<1Hz)
567 Oscillations in Thalamocortical Neurons in Vitro. Neuron 33:947–958 Available at:
568 http://www.sciencedirect.com/science/article/pii/S0896627302006232.

569 Huguenard JR, McCormick DA (2007) Thalamic synchrony and dynamic regulation of global
570 forebrain oscillations. Trends Neurosci 30:350–356.

571 Huguenard JR, Prince DA (1992) A novel T-type current underlies prolonged Ca2+-dependent
572 burst firing in GABAergic neurons of rat thalamic reticular nucleus. J Neurosci 12:3804–
573 3817.

574 Huguenard JR, Prince DA (1994) Intrathalamic rhythmicity studied in vitro: Nominal T-current
575 modulation causes robust antioscillatory effects. J Neurosci 14:5485–5502.

576 Kim U, McCormick DA (1998) Functional and ionic properties of a slow afterhyperpolarization in
577 ferret perigeniculate neurons in vitro. J Neurophysiol 80:1222–1235.

578 Kim U, Sanchez-Vives M V., McCormick DA (1997) Functional dynamics of GABAergic
579 inhibition in the thalamus. Science (80-) 278:130–134.

580 Kim YS, Kang E, Makino Y, Park S, Shin JH, Song H, Launay P, Linden DJ (2013)
581 Characterizing the conductance underlying depolarization-induced slow current in
582 cerebellar Purkinje cells. J Neurophysiol 109:1174–1181.

583 Kulkarni M, Zhang K, Kirkwood A (2011) Single-cell persistent activity in anterodorsal thalamus.
584 Neurosci Lett 498:179–184 Available at: http://dx.doi.org/10.1016/j.neulet.2011.02.051.

585 Launay P, Fleig A, Perraud AL, Scharenberg AM, Penner R, Kinet JP (2002) TRPM4 is a Ca2+-
586 activated nonselective cation channel mediating cell membrane depolarization. Cell
587 109:397–407.

588 Lee CR, Machold RP, Witkovsky P, Rice ME (2013) TRPM2 channels are required for NMDA-
589 induced burst firing and contribute to H2O2-dependent modulation in substantia nigra pars
590 reticulata GABAergic neurons. J Neurosci 33:1157–1168.

591 Lei YT, Thuault SJ, Launay P, Margolskee RF, Kandel ER, Siegelbaum SA (2014) Differential
592 contribution of TRPM4 and TRPM5 nonselective cation channels to the slow
593 afterdepolarization in mouse prefrontal cortex neurons. Front Cell Neurosci 8:1–14.

594 Lemieux M, Chen JY, Lonjers P, Bazhenov M, Timofeev I (2014) The impact of cortical
595 deafferentation on the neocortical slow oscillation. J Neurosci 34:5689–5703.

596 Lüthi A (2014) Sleep spindles: Where they come from, what they do.

597 Menigoz A, Ahmed T, Sabanov V, Philippaert K, Pinto S, Kerselaers S, Segal A, Freichel M,
598 Voets T, Nilius B, Vennekens R, Balschun D (2016) TRPM4-dependent post-synaptic
599 depolarization is essential for the induction of NMDA receptor-dependent LTP in CA1
600 hippocampal neurons. Pflugers Arch Eur J Physiol 468:593–607.

601 Mrejeru A, Wei A, Ramirez JM (2011) Calcium-activated non-selective cation currents are
602 involved in generation of tonic and bursting activity in dopamine neurons of the substantia
603 nigra pars compacta. J Physiol 589:2497–2514.

604 Neske GT (2016) The slow oscillation in cortical and thalamic networks: Mechanisms and

605 functions. Front Neural Circuits 9:1–25.

606 Neyer C, Herr D, Kohmann D, Budde T, Pape HC, Coulon P (2016) MGluR-mediated calcium
607 signalling in the thalamic reticular nucleus. Cell Calcium 59:312–323 Available at:
608 http://dx.doi.org/10.1016/j.ceca.2016.03.009.

609 Nilius B, Prenen J, Droogmans G, Voets T, Vennekens R, Freichel M, Wissenbach U, Flockerzi
610 V (2003) Voltage dependence of the Ca2+-activated cation channel TRPM4. J Biol Chem
611 278:30813–30820.

612 Nilius B, Prenen J, Voets T, Droogmans G (2004) Intracellular nucleotides and polyamines
613 inhibit the Ca2+- activated cation channel TRPM4b. Pflugers Arch Eur J Physiol 448:70–
614 75.

615 Ozhatil LC, Delalande C, Bianchi B, Nemeth G, Kappel S, Thomet U, Ross-Kaschitza D,
616 Simonin C, Rubin M, Gertsch J, Lochner M, Peinelt C, Reymons J-L, Abriel H (2018)
617 Identification of potent and selective small molecule inhibitors of the cation channel
618 TRPM4. Br J Pharmacol 175:2504–2519.

619 Picardo MCD, Sugimura YK, Dorst KE, Kallurkar PS, Akins VT, Ma X, Teruyama R, Guinamard
620 R, Kam K, Saha MS, Del Negro CA (2019) Trpm4 ion channels in pre-bötzinger complex
621 interneurons are essential for breathing motor pattern but not rhythm. PLoS Biol 17:1–30.

622 Pinault D (2004) The thalamic reticular nucleus: Structure, function and concept.

623 Pita-Almenar JD, Yu D, Lu HC, Beierlein M (2014) Mechanisms Underlying Desynchronization
624 of Cholinergic-Evoked Thalamic Network Activity. J Neurosci 34:14463–14474.

625 Pressler RT, Regehr WG (2013) Metabotropic glutamate receptors drive global persistent
626 inhibition in the visual thalamus. J Neurosci 33:2494–2506.

627 Rigas P, Castro-Alamancos MA (2007) Thalamocortical up states: Differential effects of intrinsic
628 and extrinsic cortical inputs on persistent activity. J Neurosci 27:4261–4272.

629 Riquelme D, Silva I, Philp AM, Huidobro-Toro JP, Cerda O, Trimmer JS, Leiva-Salcedo E
630 (2018) Subcellular localization and activity of TRPM4 in medial prefrontal cortex layer 2/3.
631 Front Cell Neurosci 12:1–13.

632 Sachdeva R, Schlotterer A, Schumacher D, Matka C, Mathar I, Dietrich N, Medert R, Kriebs U,
633 Lin J, Nawroth P, Birnbaumer L, Fleming T, Hammes HP, Freichel M (2018) TRPC proteins
634 contribute to development of diabetic retinopathy and regulate glyoxalase 1 activity and
635 methylglyoxal accumulation. Mol Metab 9:156–167 Available at:
636 https://doi.org/10.1016/j.molmet.2018.01.003.

637 Sanchez-Vives M V., McCormick DA (2000) Cellular and network mechanisms of rhytmic
638 recurrent activity in neocortex. Nat Neurosci 3:1027–1034.

639 Schofield CM, Kleiman-Weiner M, Rudolph U, Huguenard JR (2009) A gain in GABA A receptor
640 synaptic strength in thalamus reduces oscillatory activity and absence seizures. Proc Natl
641 Acad Sci U S A 106:7630–7635.

642 Steriade M, Contreras D, Dossi RC, Nunez A (1993a) The slow (<1 Hz) oscillation in reticular
643 thalamic and thalamocortical neurons: Scenario of sleep rhythm generation in interacting
644 thalamic and neocortical networks. J Neurosci 13:3284–3299.

645 Steriade M, Nunez A, Amzica F (1993b) A novel slow (< 1 Hz) oscillation of neocortical neurons
646 in vivo: Depolarizing and hyperpolarizing components. J Neurosci 13:3252–3265.

647 Steriade M, Nunez A, Amzica F (1993c) Intracellular analysis of relations between the slow (<1
648 Hz) neocortical oscillation and other sleep rhythms of the electroencephalogram. J

649 Neurosci.

650 Steriade M, Timofeev I (2003) Neuronal plasticity in thalamocortical networks during sleep and
651 waking oscillations. Neuron 37:563–576.

652 Stroh A, Adelsberger H, Groh A, Rühlmann C, Fischer S, Schierloh A, Deisseroth K, Konnerth A
653 (2013) Making Waves: Initiation and Propagation of Corticothalamic Ca2+ Waves In Vivo.
654 Neuron 77:1136–1150.

655 Sun Y-G, Pita-Almenar JD, Wu C-S, Renger JJ, Uebele VN, Lu H-C, Beierlein M (2013)
656 Biphasic cholinergic synaptic transmission controls action potential activity in thalamic
657 reticular nucleus neurons. J Neurosci 33:2048–2059 Available at:
658 http://www.pubmedcentral.nih.gov/articlerender.fcgi?artid=3711637&tool=pmcentrez&rend
659 ertype=abstract.

660 Sun YG, Rupprecht V, Zhou L, Dasgupta R, Seibt F, Beierlein M (2016) MGluR1 and mGluR5
661 synergistically control cholinergic synaptic transmission in the thalamic reticular nucleus. J
662 Neurosci 36:7886–7896.

663 Tian J, Zhu M (2018) GABAB Receptors Augment TRPC3-Mediated Slow Excitatory
664 Postsynaptic Current to Regulate Cerebellar Purkinje Neuron Response to Type-1
665 Metabotropic Glutamate Receptor Activation. Cells 7:90.

666 Ting JT, Daigle T, Chen Q, Feng G (2014) Acute brain slice method for adult and aging animals:
667 application of targeted patch clamp analysis and optogenetics. In: Methods in Molecular
668 Biology, Patch-Clam. (Martina M, Taverna S, eds), pp 221–242. New York: Humana Press.

669 Varga AW et al. (2016) Reduced Slow-Wave Sleep Is Associated with High Cerebrospinal Fluid
670 Aβ42 Levels in Cognitively Normal Elderly. Sleep 39:2041–2048.

671 Williams SR, Tóth TI, Turner JP, Hughes SW, Crunelli V (1997) The “window” component of the
672 low threshold Ca2+ current produces input signal amplification and bistability in cat and rat
673 thalamocortical neurones. J Physiol.

674 Yamaguchi S, Tanimoto A, Otsuguro KI, Hibino H, Ito S (2014) Negatively charged amino acids
675 near and in transient receptor potential (TRP) domain of TRPM4 channel are one
676 determinant of its Ca2+ sensitivity. J Biol Chem 289:35265–35282.

677 Zaman T, Lee K, Park C, Paydar A, Choi JH, Cheong E, Lee CJ, Shin HS (2011) CaV2.3
678 Channels Are Critical for Oscillatory Burst Discharges in the Reticular Thalamus and
679 Absence Epilepsy. Neuron 70:95–108 Available at:
680 http://dx.doi.org/10.1016/j.neuron.2011.02.042.

681 Zhang Z, Okawa H, Wang Y, Liman ER (2005) Phosphatidylinositol 4,5-Bisphosphate rescues
682 TRPM4 channels from desensitization. J Biol Chem 280:39185–39192.

683 Zhao S, Ting JT, Atallah HE, Qiu L, Tan J, Gloss B, Augustine GJ, Deisseroth K, Luo M,
684 Graybiel AM, Feng G (2011) Cell type-specific channelrhodopsin-2 transgenic mice for
685 optogenetic dissection of neural circuitry function. Nat Methods 8:745–755.

686 Zylberberg J, Strowbridge BW (2017) Mechanisms of persistent activity in cortical circuits:
687 Possible neural substrates for working memory. Annu Rev Physiol 40:60. – 627.

688

689

690

691

692

693

694 **Legends:**

695 **Figure 1. Rhythmic activity in thalamic networks. A.** Loose-patch recording of TRN neuron
696 showing rhythmic burst firing. **B.** Another TRN neuron showing rhythmic persistent firing (PF,
697 *left*), with a close-up (*right*) showing an individual bout of PF. **C.** Voltage-clamp recording of VB
698 neuron held at 0 mV displaying rhythmic bursts of IPSCs. **D.** Recording of another VB neuron
699 displaying rhythmic barrages of IPSCs (*left*). Close-up (*right*) shows a single barrage of IPSCs.
700 **E.** Summary data (n = 29) plotting the average duration of TRN firing as a function of oscillation
701 frequency. Red asterisks denote recordings shown in A and B. Dashed line marks criterion
702 separating between bursting and PF. **F.** Current clamp recording of TRN neuron, showing PF
703 during network activity. Close up (*right*) shows that bursts of EPSCs (highlighted by the red
704 arrows) trigger PF. **G.** Representative recording of rhythmic barrages of IPSCs in VB neuron,
705 under control conditions (*left*) and following bath application of NBQX (10 μM, *right*). Similar
706 data were obtained from 4 other VB neurons.

707 **Figure 2. Axonal divergence and convergence characterize TRN outputs to VB.** VB
708 recordings were performed in voltage clamp, with cells held at 0 mV. **A.** Divergent TRN output
709 to VB neurons. Dual recordings of neighboring VB cells showing a single barrage of IPSCs, with
710 a close-up (*middle*) highlighting precise synchrony of individual IPSCs activity in both cells.
711 Traces are normalized to the initial IPSC amplitude for both recordings. Schematic (*right*)
712 outlines proposed divergent TRN projections giving rise to VB responses. **B.** Convergent TRN
713 input to VB neuron**.** (*left*) Voltage-clamp recording of VB neuron with IPSC bursts (red tick
714 marks) and prolonged IPSC barrages (cyan tick marks) with distinct initial amplitudes. Close-up
715 (*middle*) shows overlay of individual events**.** Schematic (*right*) indicates proposed circuits giving

716 rise to VB response. **C.** Another example of TRN convergence onto VB neuron. (*left*) Recording
717 of VB neuron showing IPSC barrages with two distinct initial amplitudes (green and purple tick
718 marks, respectively). Close-up (*middle*) shows overlay of individual events**.** Schematic (*right*)
719 indicates proposed circuits giving rise to VB response.

720 **Figure 3. PF is developmentally regulated and is controlled by SK conductances. A.** Brief
721 depolarizing current steps (25 ms, 400 pA, RMP = -75 mV) lead to two distinct firing patterns,
722 Persistent Firing (PF, *top*) or Burst Firing (Bu, *bottom*). **B.** Summary data (n = 111) showing
723 bimodal distribution of current-step evoked membrane depolarizations. Grey line indicates
724 criterion separating PF and Bu. **C.** Raster plot of AP activity in representative TRN neuron
725 showing rundown of PF. **D.** Representative recordings of TRN neurons with PF at three
726 developmental stages, in control conditions (*black*) and in the presence of apamin (500 nM,
727 *red*). **E.** Summary data showing incidence of PF across development (P13-18: n = 24 in control,
728 n = 25 in apamin; P28-38: n = 23 in control, n = 22 in apamin; P90-120: 111 in control, n = 50 in
729 apamin). **F.** For the same cells as in D, summary data quantifying membrane potential duration
730 for all TRN cells across development, in control conditions and in apamin.

731 **Figure 4. T-type Ca^{2+} channels but not mGluRs are required for PF. A.** Representative
732 recordings of PF from two different TRN neurons, in control conditions and in the presence of
733 the mGluR1 antagonist JNJ 16259685 (1 μM) and the mGluR5 antagonist MTEP (10 μM). **B.**
734 Summary data quantifying duration of evoked membrane depolarization in control (n = 111) and
735 in the presence of mGluR 1/5 antagonists (n = 23). **C.** Representative recording of neuron with
736 PF, initially held at a holding potential of -60 mV and then at -75 mV. **D.** Summary data
737 quantifying evoked depolarization duration as a function of holding potential for TRN cells (n =
738 15). **E.** Representative recordings in the presence of apamin and in the presence of apamin and
739 the T-type Ca^{2+} channel antagonist TTA-P2. **F.** Summary data quantifying evoked depolarization
740 duration (n = 50 in apamin, n = 17 in apamin + TTA-P2).

741

742 **Figure 5. A TTX-insensitive sodium current generates plateau potentials.** All recordings
743 were performed in the presence of apamin. **A.** Representative TRN recordings in the presence
744 of the L-type Ca^{2+} channel antagonist nimodipine (20 μM, *top*), in TTX (500 nM, *middle*), and in
745 the presence of TTX and NMDG replacing extracellular Na^{+} (*bottom*). **B.** Summary data
746 showing incidence of PF in the presence of nimodipine (n = 10), the P/Q- and N-type Ca^{2+}
747 channel antagonist ω-conotoxin MVIIC (1 μM, n = 10), TTX (n = 16), and TTX and NMDG (n =
748 28). Dashed line indicates incidence of PF in apamin. **C.** Summary data from the same cells as
749 in B quantifying evoked depolarization duration in each condition. Grey solid line represents
750 criterion for PF.

751 **Figure 6. TRPM4 conductances mediate PF.** All recordings were performed in the presence
752 of apamin. **A.** Representative recordings in control and in the presence of the non-selective
753 transient potential receptor (TRP) channel antagonist flufenamic acid (FFA, 100 μM, *top*), the
754 TRPM4 antagonist CBA (50 μM, *middle*), and in 2 mM $BaCl_2$ replacing extracellular $CaCl_2$
755 (*bottom*). **B.** Summary data showing incidence of PF in TRPC3 KO (KO, n = 10 cells) in
756 TRPC1,4,5,6 quadruple KO (QKO, n = 10 cells), FFA (n = 17), the non-selective TRP channel
757 antagonist 2-APB (50 μM, n = 10), the TRPM4/5 antagonists 9-phenthranol (100 μM, n = 15)
758 and glibenclamide (100 μM, n = 21), CBA (n = 15), and Ba^{2+}, (n = 15). Grey dashed line
759 represents incidence of PF in apamin. **C.** For the same cells as in B, summary data quantifying
760 the evoked depolarization duration.

761 **Figure 7. Synaptic recruitment of muscarinic AChRs suppresses PF.** Recordings were
762 carried out in slices of ChAT-ChR2-EYFP BAC mice. **A.** Loose-patch recording of a TRN neuron
763 showing brief barrage of ACh-evoked activity (*black*), which is prolonged following application of
764 the mAChR antagonist atropine (10 μM, *blue*). **B.** Raster plot of ACh-evoked neuronal activity
765 prior to and following atropine application, for the cell shown in A. **C.** Summary data quantifying

766 the average duration of ACh-evoked action potential activity before and after atropine

767 application (n = 5).

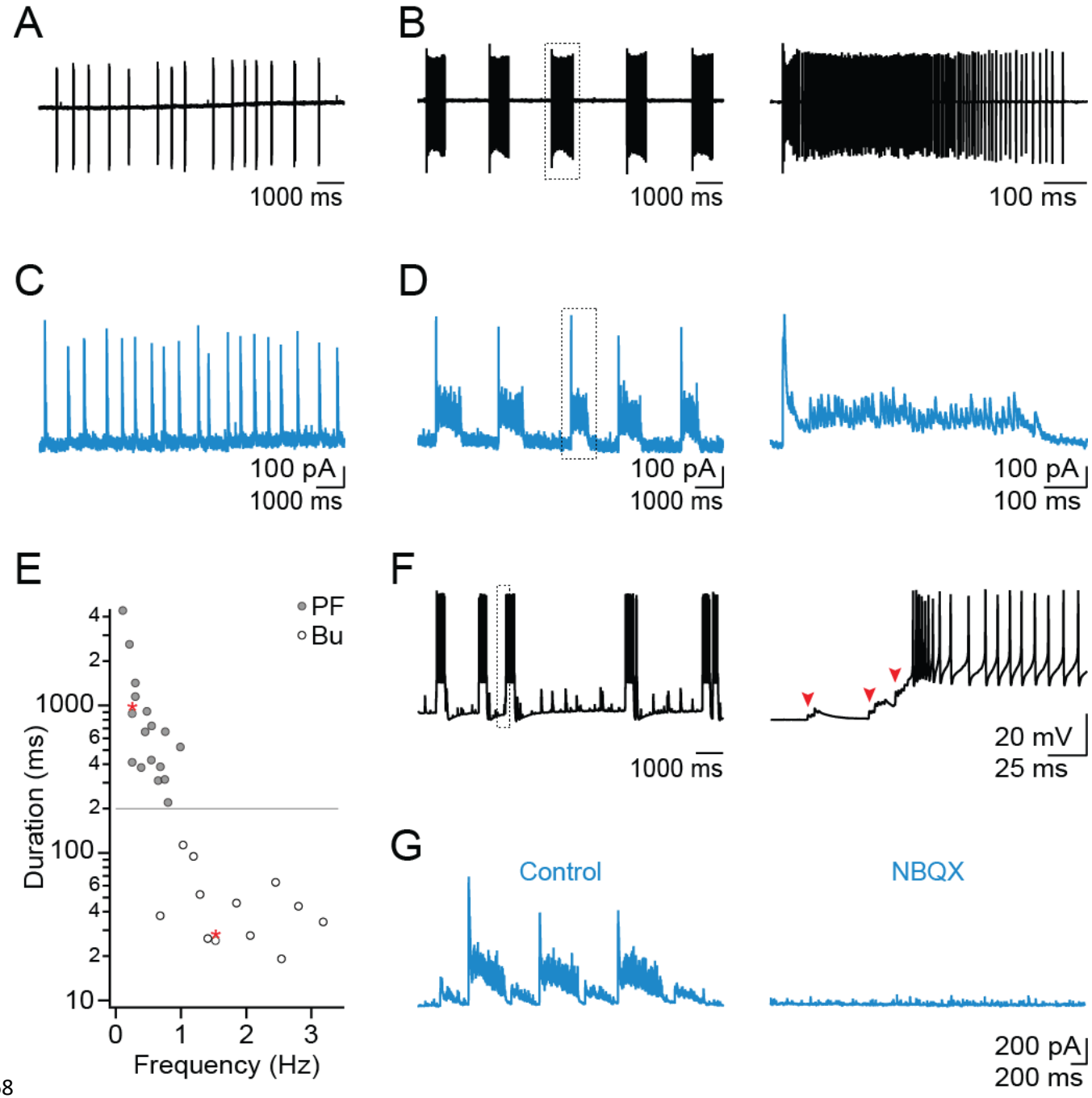

Figure 1. Rhythmic activity in thalamic networks. A. Loose-patch recording of TRN neuron showing rhythmic burst firing. **B.** Another TRN neuron showing rhythmic persistent firing (PF, *left*), with a close-up (*right*) showing an individual bout of PF. **C.** Voltage-clamp recording of VB neuron held at 0 mV displaying rhythmic bursts of IPSCs. **D.** Recording of another VB neuron displaying rhythmic barrages of IPSCs (*left*). Close-up (*right*) shows a single barrage of IPSCs. **E.** Summary data (n = 29) plotting the average duration of TRN firing as a function of oscillation frequency. Red asterisks denote recordings shown in A and B. Dashed line marks criterion separating between bursting and PF. **F.** Current clamp recording of TRN neuron, showing PF during network activity. Close up (*right*) shows that bursts of EPSCs (highlighted by the red arrows) trigger PF. **G.** Representative recording of rhythmic barrages of IPSCs in VB neuron,

779 under control conditions (*left*) and following bath application of NBQX (10 μM, *right*). Similar
780 data were obtained from 4 other VB neurons.

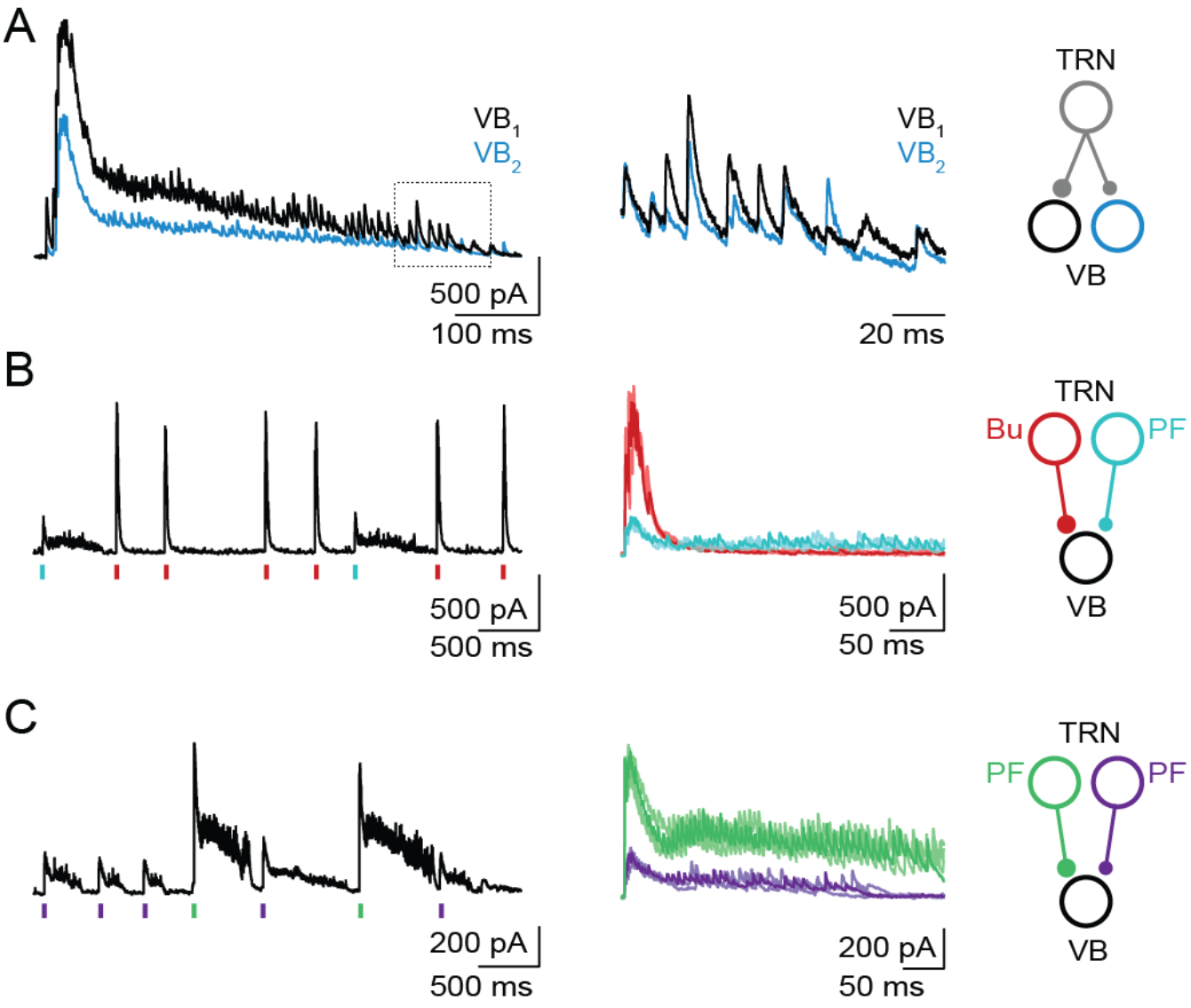

781

782 **Figure 2. Axonal divergence and convergence characterize TRN outputs to VB.** VB
783 recordings were performed in voltage clamp, with cells held at 0 mV. **A.** Divergent TRN output
784 to VB neurons. Dual recordings of neighboring VB cells showing a single barrage of IPSCs, with
785 a close-up (*middle*) highlighting precise synchrony of individual IPSCs activity in both cells.
786 Traces are normalized to the initial IPSC amplitude for both recordings. Schematic (*right*)
787 outlines proposed divergent TRN projections giving rise to VB responses. **B.** Convergent TRN
788 input to VB neuron**.** (*left*) Voltage-clamp recording of VB neuron with IPSC bursts (red tick
789 marks) and prolonged IPSC barrages (cyan tick marks) with distinct initial amplitudes. Close-up
790 (*middle*) shows overlay of individual events**.** Schematic (*right*) indicates proposed circuits giving
791 rise to VB response. **C.** Another example of TRN convergence onto VB neuron. (*left*) Recording
792 of VB neuron showing IPSC barrages with two distinct initial amplitudes (green and purple tick
793 marks, respectively). Close-up (*middle*) shows overlay of individual events**.** Schematic (*right*)
794 indicates proposed circuits giving rise to VB response.

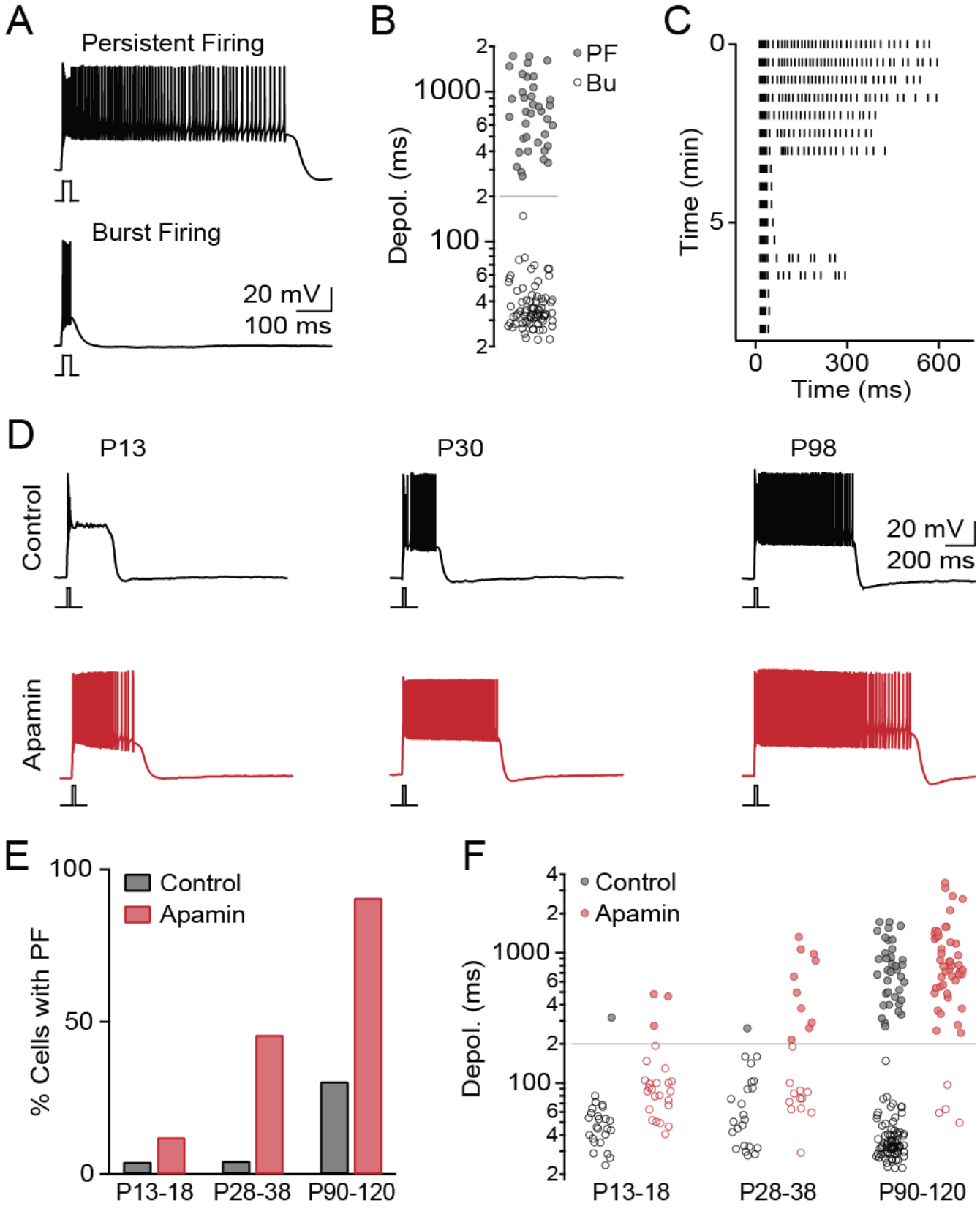
A
Persistent Firing
Burst Firing
20 mV
100 ms
B
PF
Bu
Depol. (ms)
1000
100
C
Time (min)
0
5
0
300
600
Time (ms)
D
P13
P30
P98
Control
Apamin
20 mV
200 ms
E
Control
Apamin
% Cells with PF
100
50
0
P13-18
P28-38
P90-120
F
Control
Apamin
Depol. (ms)
1000
100
P13-18
P28-38
P90-120

795

Figure 3. PF is developmentally regulated and is controlled by SK conductances. A. Brief depolarizing current steps (25 ms, 400 pA, RMP = -75 mV) lead to two distinct firing patterns, Persistent Firing (PF, *top*) or Burst Firing (Bu, *bottom*). **B.** Summary data (n = 111) showing bimodal distribution of current-step evoked membrane depolarizations. Grey line indicates criterion separating PF and Bu. **C.** Raster plot of AP activity in representative TRN neuron showing rundown of PF. **D.** Representative recordings of TRN neurons with PF at three developmental stages, in control conditions (*black*) and in the presence of apamin (500 nM, *red*). **E.** Summary data showing incidence of PF across development (P13-18: n = 24 in control, n = 25 in apamin; P28-38: n = 23 in control, n = 22 in apamin; P90-120: 111 in control, n = 50 in apamin). **F.** For the same cells as in D, summary data quantifying membrane potential duration for all TRN cells across development, in control conditions and in apamin.

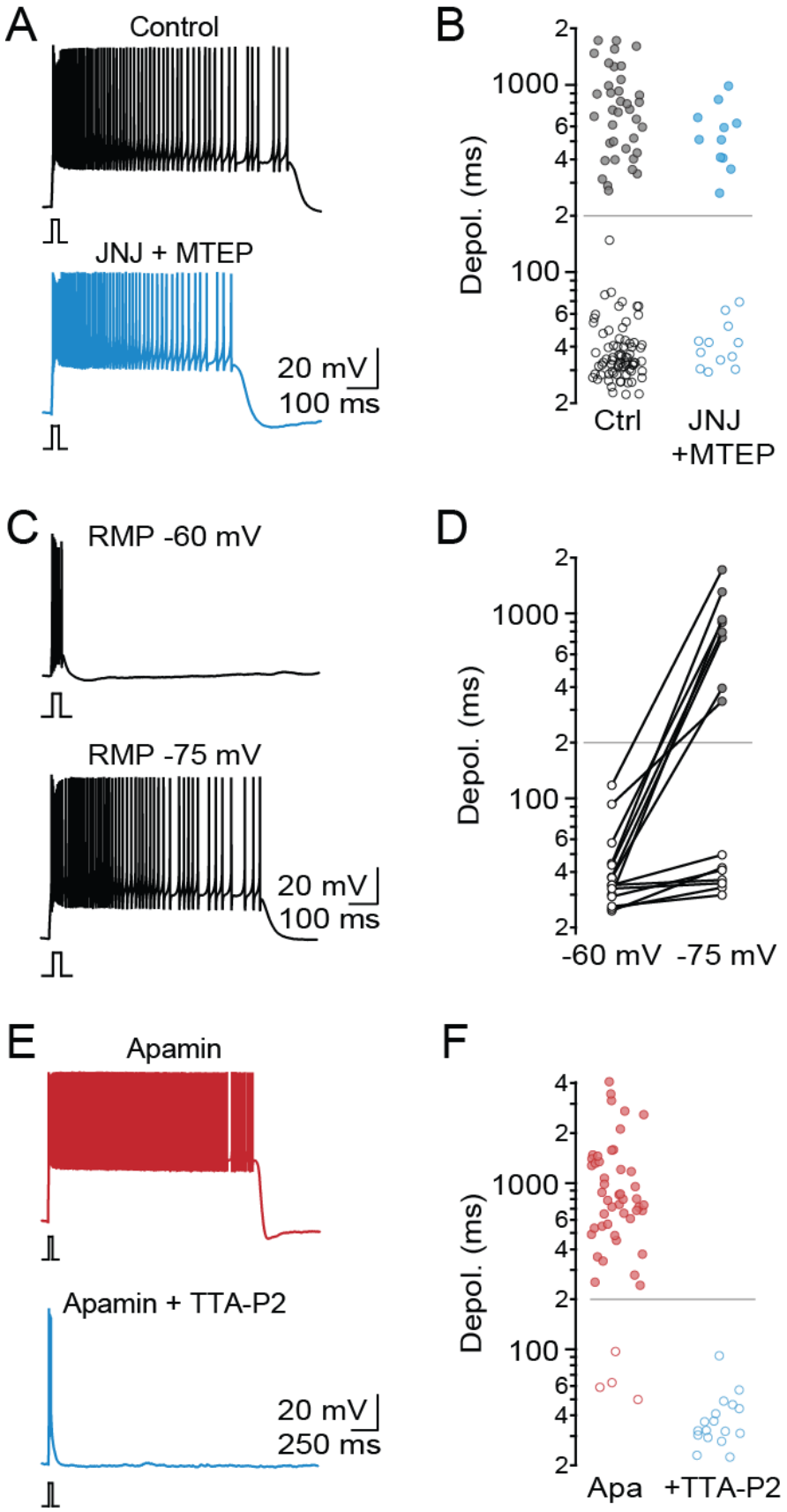
A
Control
JNJ + MTEP
20 mV
100 ms
B
Depol. (ms)
Ctrl
JNJ
+MTEP
C
RMP -60 mV
RMP -75 mV
20 mV
100 ms
D
Depol. (ms)
-60 mV
-75 mV
E
Apamin
Apamin + TTA-P2
20 mV
250 ms
F
Depol. (ms)
Apa
+TTA-P2

807

808 **Figure 4. T-type Ca^{2+} channels but not mGluRs are required for PF. A.** Representative
809 recordings of PF from two different TRN neurons, in control conditions and in the presence of
810 the mGluR1 antagonist JNJ 16259685 (1 μM) and the mGluR5 antagonist MTEP (10 μM). **B.**
811 Summary data quantifying duration of evoked membrane depolarization in control (n = 111) and
812 in the presence of mGluR 1/5 antagonists (n = 23). **C.** Representative recording of neuron with
813 PF, initially held at a holding potential of -60 mV and then at -75 mV. **D.** Summary data
814 quantifying evoked depolarization duration as a function of holding potential for TRN cells (n =
815 15). **E.** Representative recordings in the presence of apamin and in the presence of apamin and
816 the T-type Ca^{2+} channel antagonist TTA-P2. **F.** Summary data quantifying evoked depolarization
817 duration (n = 50 in apamin, n = 17 in apamin + TTA-P2).

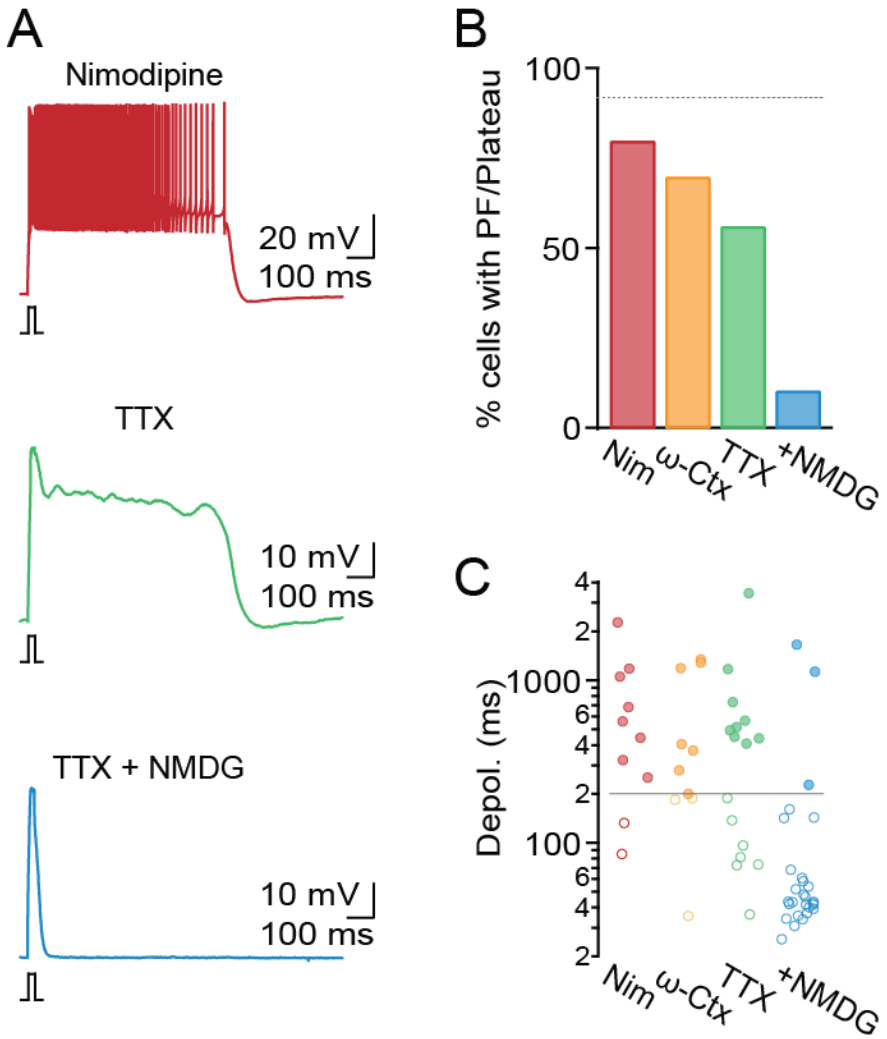

Figure 5. A TTX-insensitive sodium current generates plateau potentials. All recordings were performed in the presence of apamin. **A.** Representative TRN recordings in the presence of the L-type Ca^{2+} channel antagonist nimodipine (20 μM, *top*), in TTX (500 nM, *middle*), and in the presence of TTX and NMDG replacing extracellular Na^{+} (*bottom*). **B.** Summary data showing incidence of PF in the presence of nimodipine (n = 10), the P/Q- and N-type Ca^{2+} channel antagonist ω-conotoxin MVIIC (1 μM, n = 10), TTX (n = 16), and TTX and NMDG (n = 28). Dashed line indicates incidence of PF in apamin. **C.** Summary data from the same cells as in B quantifying evoked depolarization duration in each condition. Grey solid line represents criterion for PF.

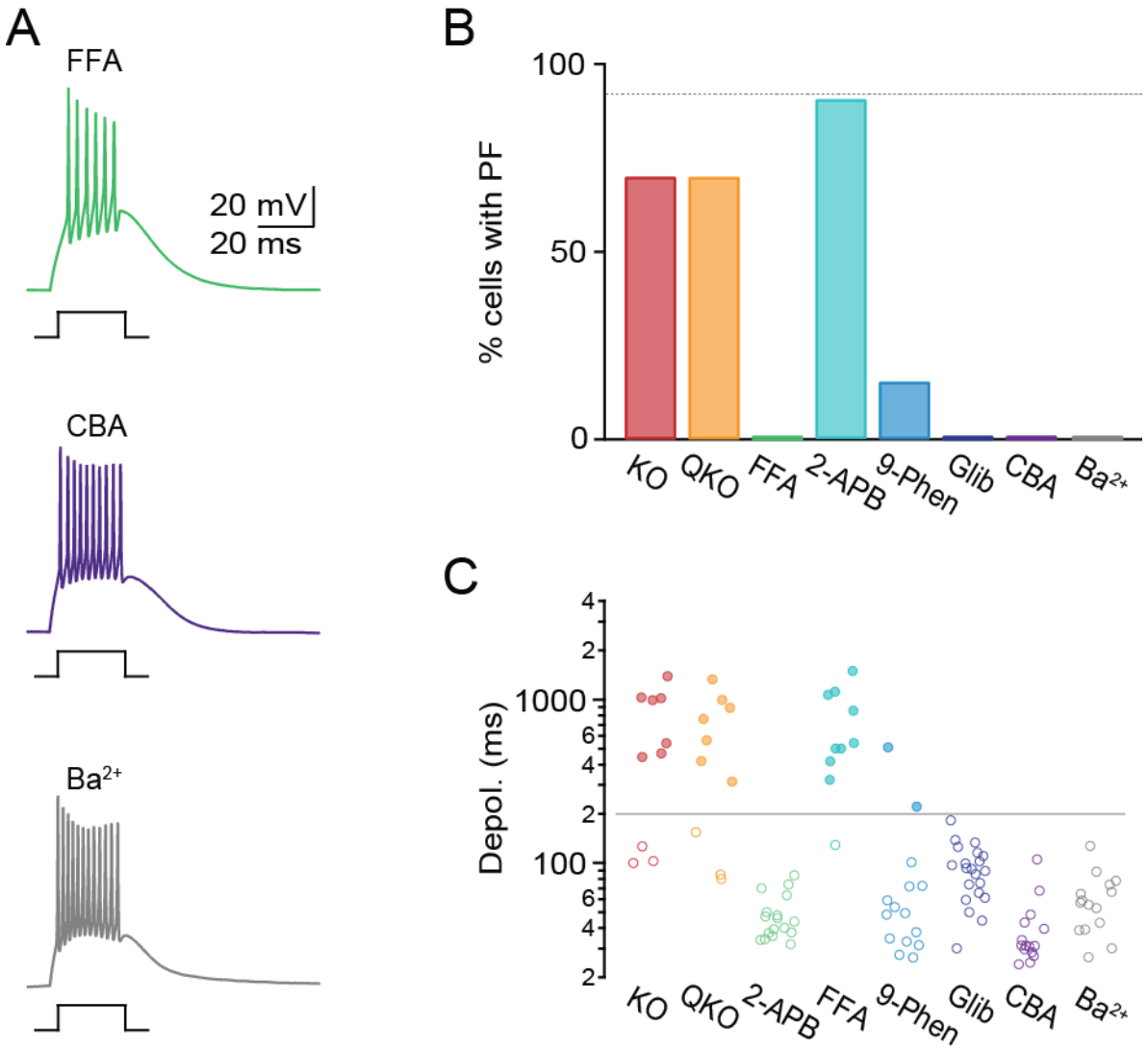

Figure 6. TRPM4 conductances mediate PF. All recordings were performed in the presence of apamin. **A.** Representative recordings in control and in the presence of the non-selective transient potential receptor (TRP) channel antagonist flufenamic acid (FFA, 100 μM, *top*), the TRPM4 antagonist CBA (50 μM, *middle*), and in 2 mM $BaCl_2$ replacing extracellular $CaCl_2$ (*bottom*). **B.** Summary data showing incidence of PF in TRPC3 KO (KO, n = 10 cells) in TRPC1,4,5,6 quadruple KO (QKO, n = 10 cells), FFA (n = 17), the non-selective TRP channel antagonist 2-APB (50 μM, n = 10), the TRPM4/5 antagonists 9-phenthranol (100 μM, n = 15) and glibenclamide (100 μM, n = 21), CBA (n = 15), and Ba^{2+}, (n = 15). Grey dashed line represents incidence of PF in apamin. **C.** For the same cells as in B, summary data quantifying the evoked depolarization duration.

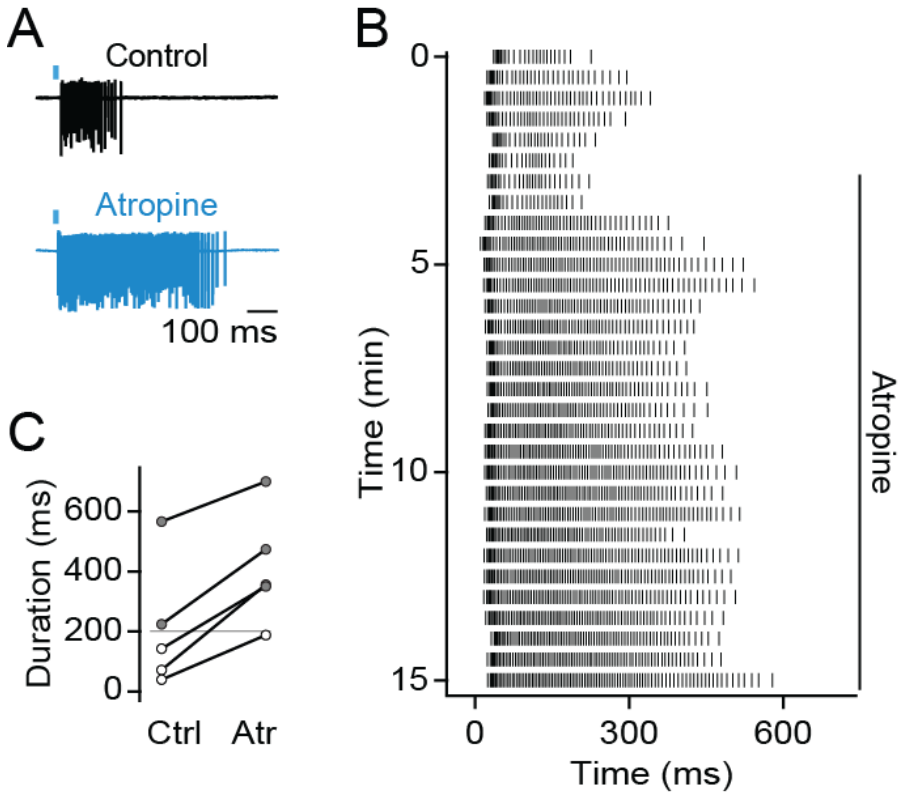

841

842 **Figure 7. Synaptic recruitment of muscarinic AChRs suppresses PF.** Recordings were
843 carried out in slices of ChAT-ChR2-EYFP BAC mice. **A.** Loose-patch recording of a TRN neuron
844 showing brief barrage of ACh-evoked activity (*black*), which is prolonged following application of
845 the mAChR antagonist atropine (10 μM, *blue*). **B.** Raster plot of ACh-evoked neuronal activity
846 prior to and following atropine application, for the cell shown in A. **C.** Summary data quantifying
847 the average duration of ACh-evoked action potential activity before and after atropine
848 application (n = 5).